

Supporting Information

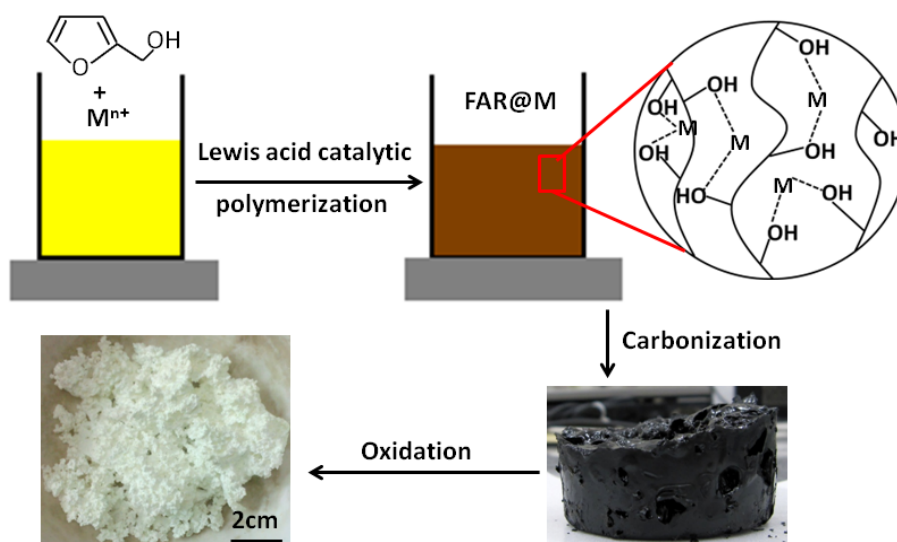
Large-Scale, Three-Dimensional, Free-Standing, and Mesoporous Metal Oxide Networks for High-Performance Photocatalysis

Hua Bai, Xinshi Li, Chao Hu, Xuan Zhan, Junfang Li, Yan Yan, and Guangcheng Xi*

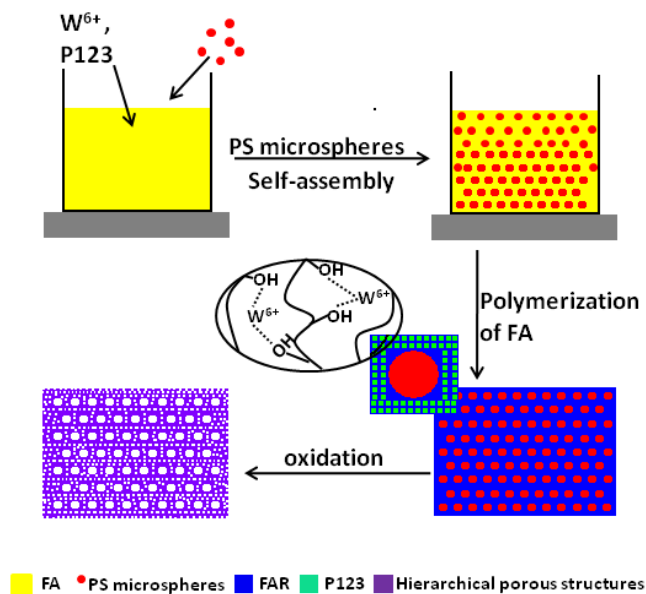
Inspection and Research Center of Nanomaterials and Nanoproducts, Chinese Academy of Inspection and Quarantine, No. A3, North Route, Gaobeidian, Chaoyang District, Beijing, 100123, P. R. China

*(Guangcheng Xi) Email: xiguangcheng@caiq.gov.cn

Supporting Figures



Scheme S1. Schematic procedure for the formation of the 3D mesoporous SnO₂ networks, $M^{n+} = \text{Sn}^{4+}$.



Scheme S2. Schematic procedure for the formation of the 3D HMM WO_3 networks.

Table 1. The specific surface area and pore size of the samples.

Sample	Phase	$S_{\text{BET}}^{[a]}$ [m^2g^{-1}]	$r_{\text{pore}}^{[b]}$ [nm]	$V_{\text{pore}}^{[c]}$ [cm^3g^{-1}]
SnO_2	rutile	185	8.3	0.31
WO_3	monoclinic	130	8.6	0.14
Fe_2O_3	$\alpha\text{-Fe}_2\text{O}_3$	155	6.5	0.25
Co_3O_4	cubic	170	6.8	0.29
NiO	cubic	96	7.8	0.19
CuO	monoclinic	119	6.8	0.20
CeO_2	cubic	114	7.9	0.22

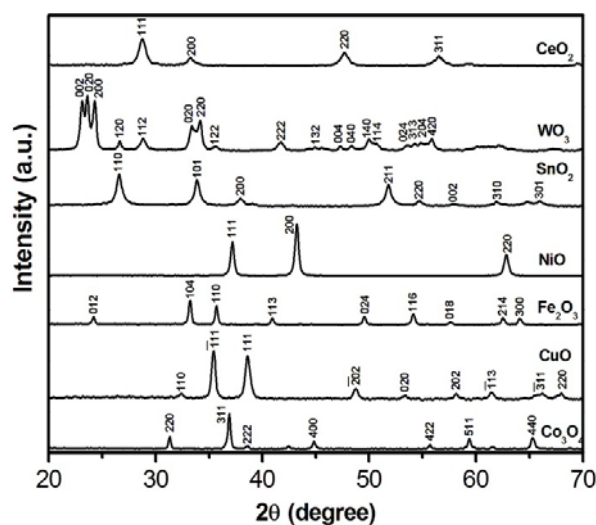


Figure S1. XRD patterns of the as-synthesized samples, including CeO_2 , WO_3 , SnO_2 , Fe_2O_3 , NiO , Co_3O_4 , CuO .

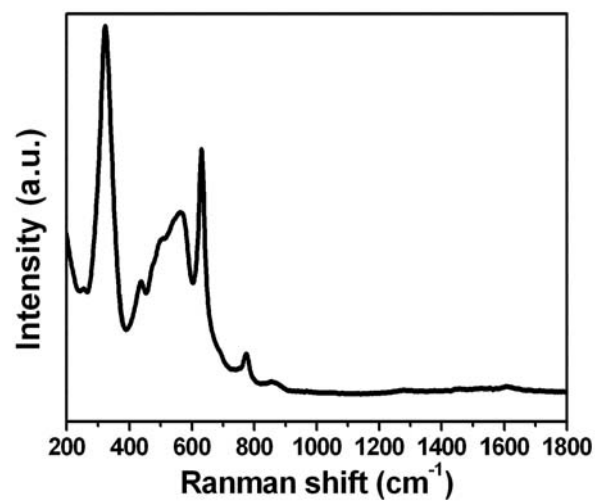


Figure S2. Raman spectrum of the as-synthesized 3D porous SnO₂ networks.

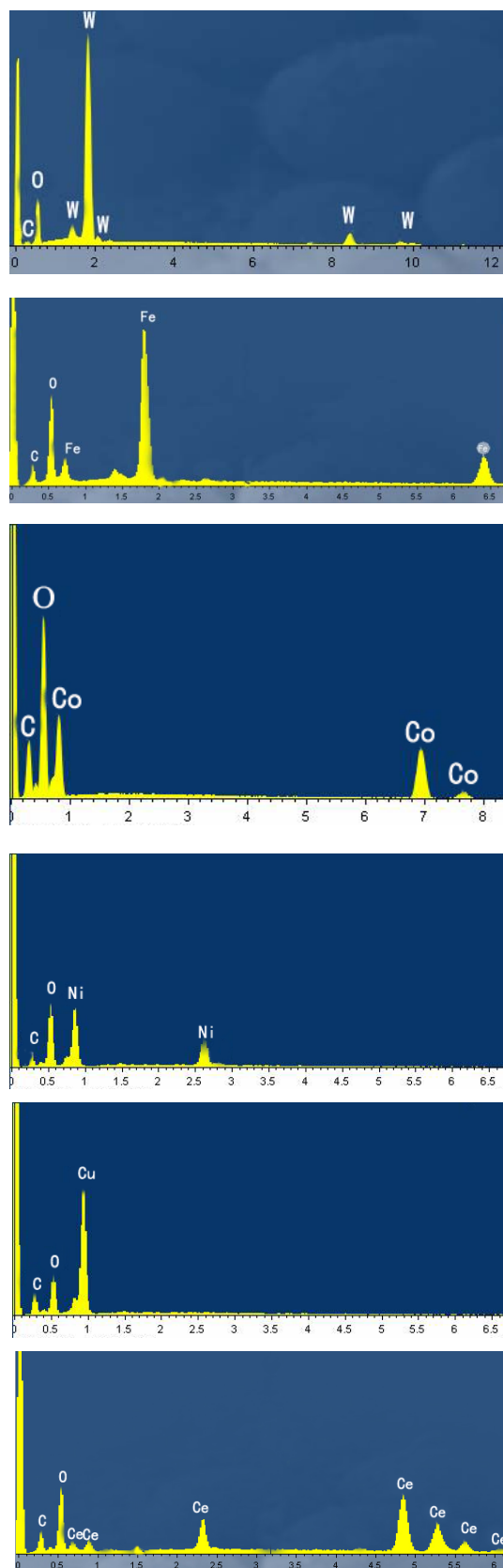


Figure S3. The energy–dispersion X–Ray spectroscopy (EDS) of the as-synthesized WO₃, Fe₂O₃, Co₃O₄, NiO, CuO, and CeO₂.

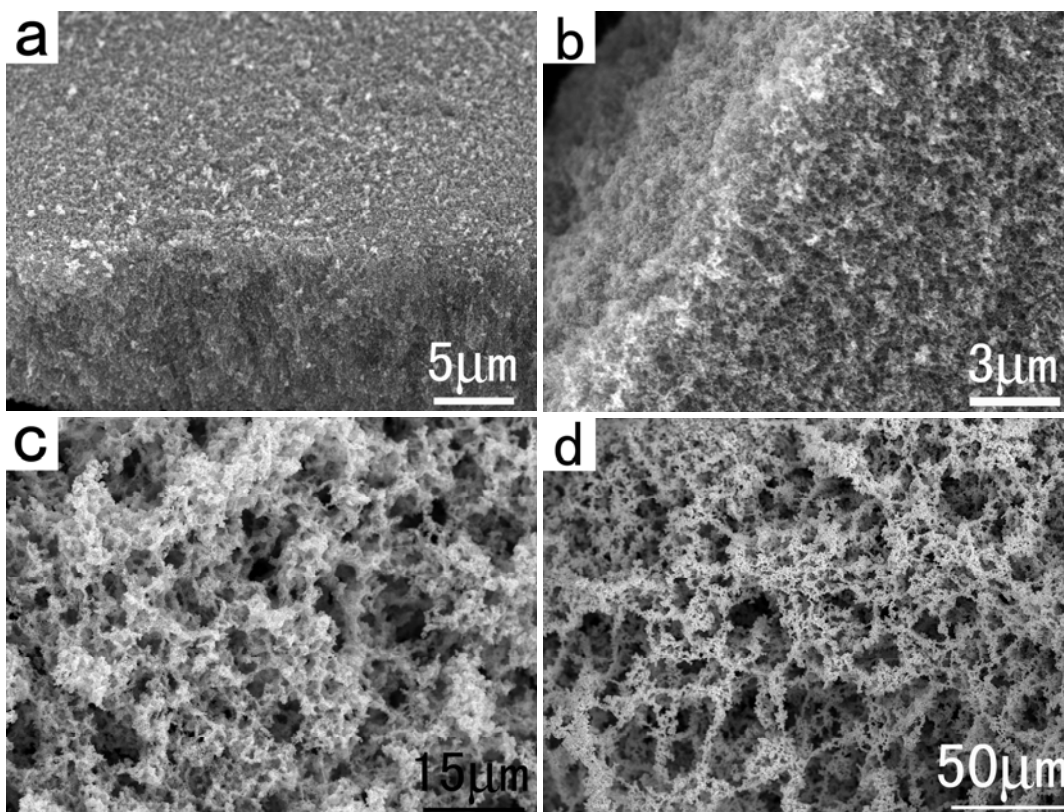


Figure S4. The typical SEM images of the free-standing 3D porous WO_3 networks obtained with different amount of FA: (a) 15 mL, (b) 25 mL, (c) 35 mL, and (d) 45 mL.

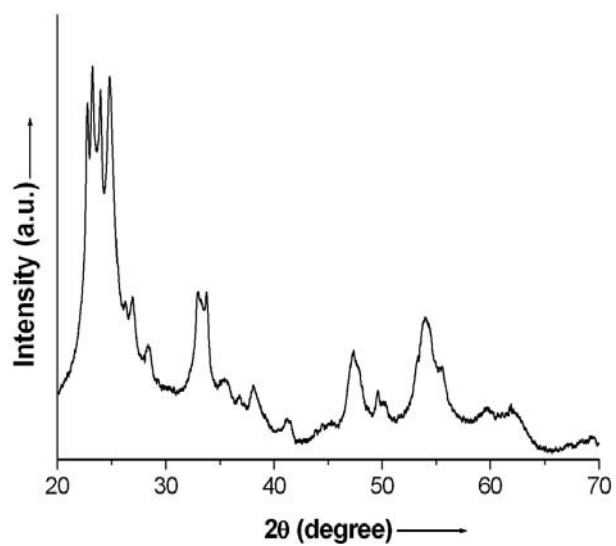


Figure S5. XRD pattern of the as-synthesized 3D mesoporous TiO_2/WO_3 hybrid networks.

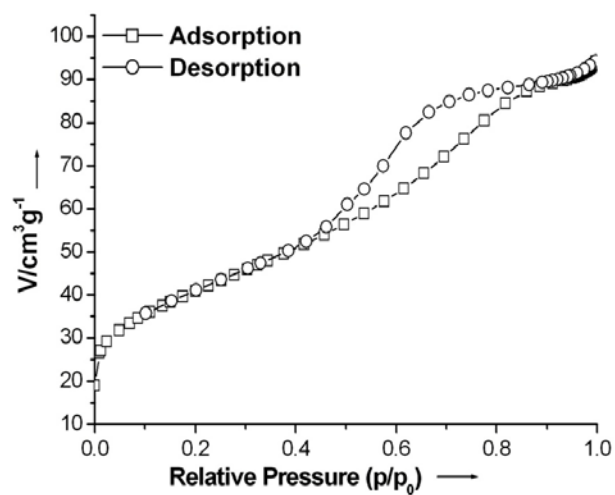


Figure S6. Nitrogen adsorption–desorption isotherm plot for the 3D mesoporous TiO_2/WO_3 networks. Inset: Barrett–Joyner–Halenda (BJH) pore–size distribution plot of the 3D mesoporous TiO_2/WO_3 sample.

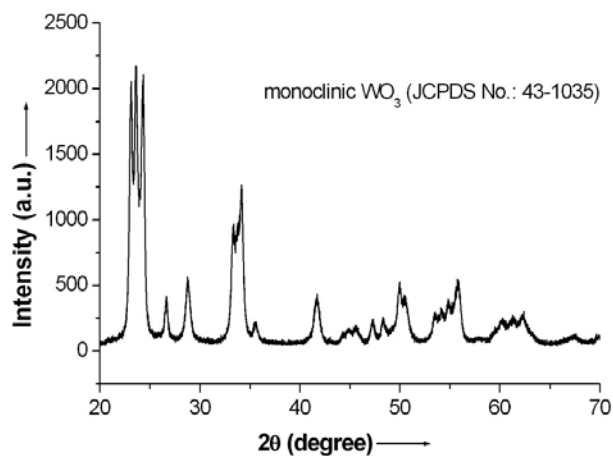


Figure S7. The typical XRD pattern of the as–obtained 3D macro/mesoporous WO_3 sample.

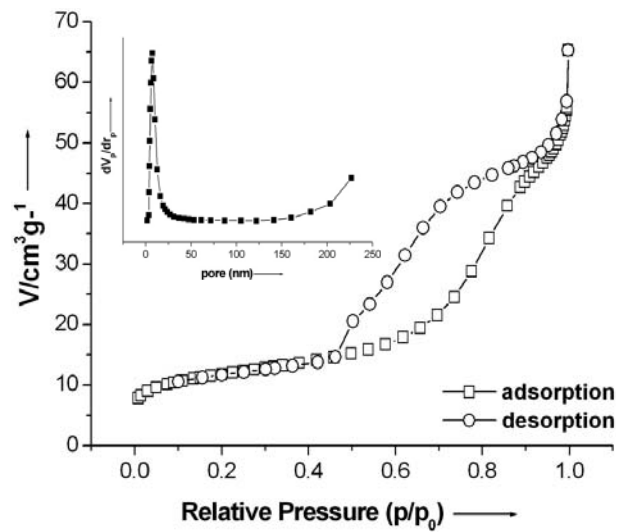


Figure S8. Nitrogen adsorption–desorption isotherm plot of the 3D macro/mesoporous WO_3 sample. Inset: Barrett–Joyner–Halenda (BJH) pore–size distribution plot of the 3D macro/mesoporous WO_3 sample.

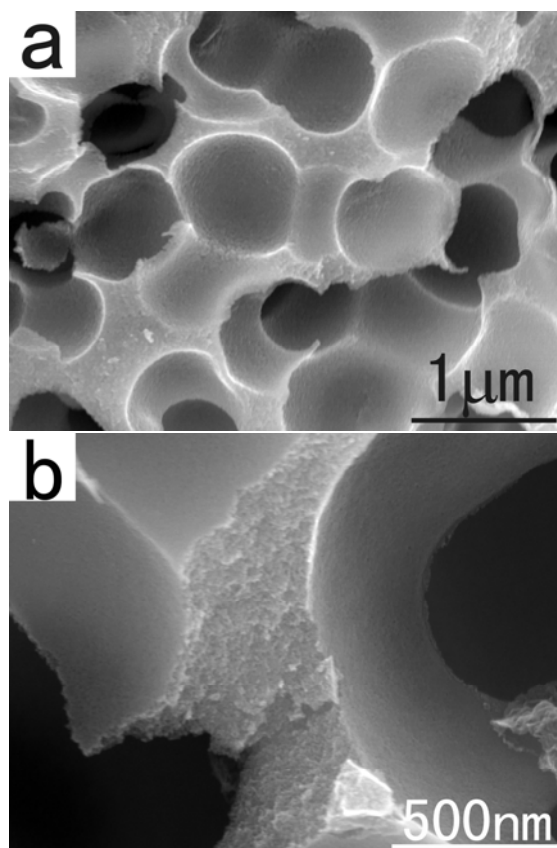


Figure S9. SEM images of the HMM WO_3 networks with thick walls.

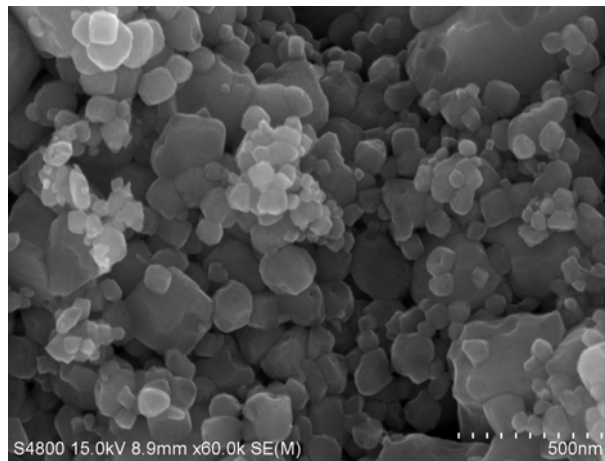


Figure S10. SEM image of the commercial WO₃ particles.

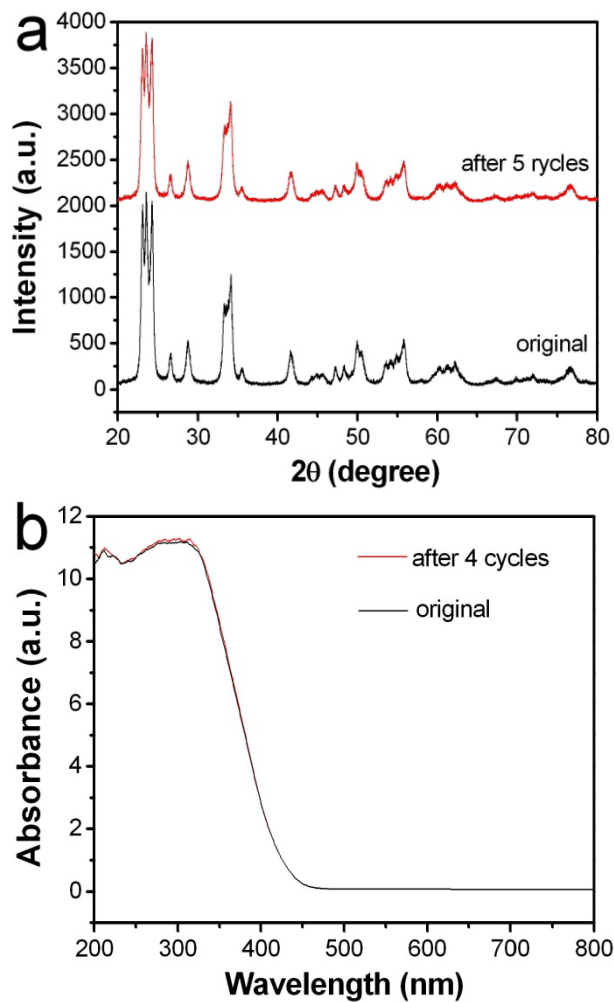


Figure S11. XRD pattern (a) and UV-vis absorption spectra (b) of the samples after photocatalytic degradation reactions.

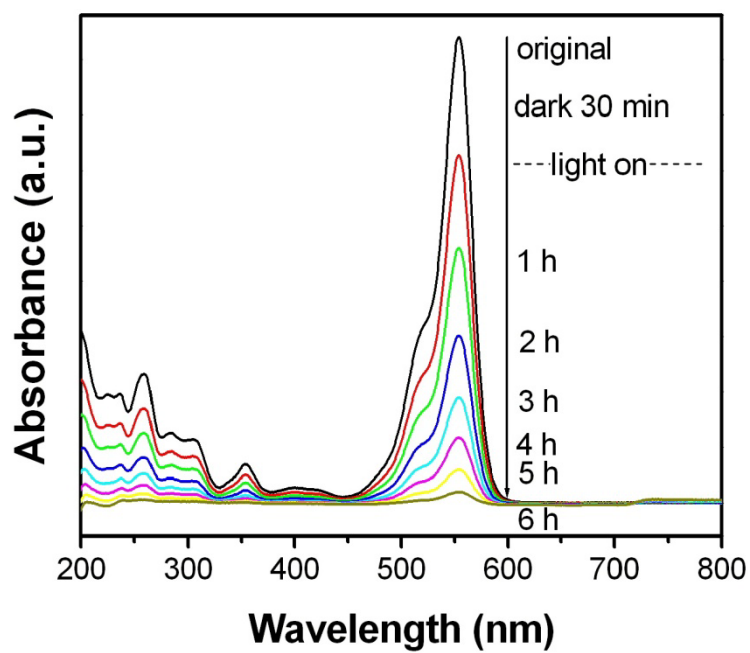


Figure S12. UV/Vis spectroscopic changes of an aqueous solution of RhB upon visible-light irradiation in the presence of the 3D mesoporous WO_3 nanomaterials. Reaction conditions: RhB concentration 10 mg/L, catalyst concentration 0.5 g/L, initial pH 6.85, sunlight with a reaction temperature of 30 °C.